A Real-Time Selective Harmonic Elimination Based on a Transient-Free Inner Closed-Loop Control for Cascaded Multilevel Inverters

Hui Zhao, *Student Member, IEEE*, Tian Jin, Shuo Wang, *Senior Member, IEEE*, and Liang Sun

***Abstract*—Applying the selective harmonic elimination (SHE) technique to grid-connected-cascaded modular multilevel inverters has been widely discussed in the literature. However, due to the difficulties of solving high-order nonlinear transcendental equations, the SHE technique cannot be implemented in real time so its applications are limited. This paper presents a technique to convert the nonlinear equations to a specific control system and use a look-up table, integral controllers and a decoupling controller to help the system converge to a zero-error steady state. An inner instantaneous observer is introduced to directly extract the harmonic spectrum of the output voltages without applying FFT algorithm to output step voltage waveforms. It can not only simplify software design but also eliminate the phase delay generated by conventional spectrum extracting algorithm. The proposed technique can achieve an accurate switching angle control and a fast response. Simulation and experimental results verified that the system can achieve zero-error steady state within one line period.**

***Index Terms*— Cascaded multilevel inverters, instantaneous observer, real-time calculation, selective harmonic elimination (SHE), zero-error steady state.**

I. Introduction

CASCADED multilevel inverters (CMI) have drawn much attention in recent years, especially in medium and high voltage applications, such as traction, high-voltage direct current electric power transmission system and wind energy interconnections because of its low switching frequencies and the capability to withstand high voltage [1], [2]. Recently, it also draws much attention from high efficiency PV inverter applications because its low switching loss. Fig. 1 shows an example of a seven-level, three-cell CMI. To reduce the harmonics injected to the power grid, the selected harmonic elimination (SHE) has been widely investigated [3]–[5].

SHE is used to optimize switching angles so as to eliminate certain orders of harmonics [3]. One of the biggest difficulties to implement SHE is solving the nonlinear equations with transcendental features [1], [5]–[7] in a DSP.

The complete solutions of SHE can be found in [3]. A method converting the transcendental equations to specific high-order polynomial equations is proposed in [3]. However, the high order equation set is still hard to solve and it becomes even harder when more number of CMI are cascaded.

Numerical solutions such as Newton–Raphson iteration and generic-algorithm-based methods (GA) are discussed in [8]. The initial values are usually very important to these numerical methods but they are very difficult to determine. In addition, the convergence of the numerical methods and the time consumed by iterations are hard to identify.

Methods like using polynomial curve fitting and interpolation to derive switching angles are discussed in [2]. These methods only generate approximate switching angle solutions. The spectrum errors caused by the switching angle errors are hard to determine; so zero steady-state error cannot be guaranteed. Techniques based on simplified equations or equal area citations can generate real-time solutions; however, zero steady-state error cannot be achieved [9] and numerical solution is still needed [5], [7].

So far, the most common way to implement SHE is still to calculate switching angles offline, store them in a look-up table (LUT), and read them based on the voltage reference of the fundamental during real-time operations. Because the stored switching angles are not continuous, the accuracy of output voltage is limited. To achieve a good accuracy, large memory space is needed. It greatly increases cost.

In this paper, the small signal and average models of CMI are first investigated for SHE. The limitations of the models are identified. Instead of solving nonlinear equations in math domain, this paper converts the equation set to a control system. The equation set can be solved by the designing of a controller to achieve desired steady state and dynamic responses. An instantaneous observer is introduced to get spectrum from switching angles without using Fourier analysis. It reduces phase delay, reduces response time and improves stability. The system's stability is analyzed using the indirect method of Lyapunov. The errors of small signal models are evaluated and the dynamic response of the system is analyzed based on the small signal model. A small LUT is employed in a feed-forward path to provide initial values so as to achieve a fast dynamic response and ensure that the system is so close to a steady state that small signal model can be applied during the dynamic response. This paper takes the three-cell CMI in Fig. 1 as an example to eliminate third and fifth harmonics in all analysis and experiments.

Manuscript received July 21, 2014; revised November 12, 2014 and January 23, 2015; accepted March 1, 2015. Date of publication March 16, 2015; date of current version September 29, 2015. This work was supported by the National Science Foundation under Award 1151126. Recommended for publication by Associate Editor B. Choi.

H. Zhao and S. Wang are with the Department of Electrical and Computer Engineering, University of Florida, Gainesville, FL 32611 USA (e-mail: zhaohui@ufl.edu; shuowang@ieee.org).

T. Jin and L. Sun are with the Department of Electrical and Computer Engineering, University of Texas at San Antonio, San Antonio, TX 78249 USA (e-mail: tianjin47@gmail.com; solbuaa@gmail.com).

Color versions of one or more of the figures in this paper are available online at http://ieeexplore.ieee.org.

Digital Object Identifier 10.1109/TPEL.2015.2413898

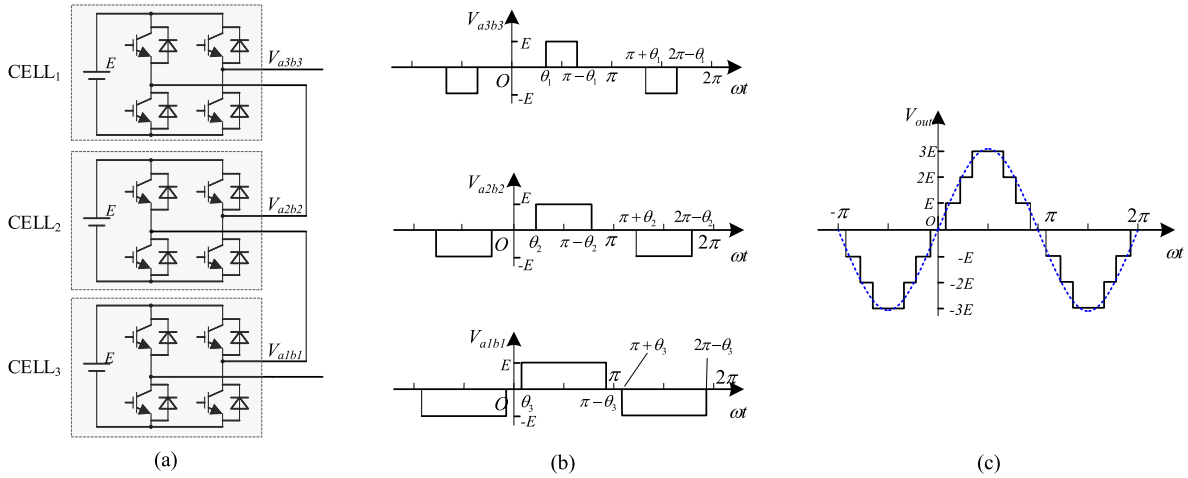

Fig. 1. Topology and waveforms of a three-cell CMI. (a) Topology of a seven-level CMI. (b) Output voltage of one cell. (c) Overall output voltage waveform.

The three-cell CMI can also be used to eliminate other order of harmonics such as fifth and seventh. The proposed technique can be applied to the CMI with any number of cells. It is well known that, with more number of cells, CMI can eliminate more orders of harmonics.

This paper is organized as follows. In Section II, the average and small signal models are developed. Their limitations are discussed. In Section III, the transcendental equation set is converted to a controlled system. The procedure to design a feedback loop including integral controllers, an inner observer and a LUT is proposed. The system stability is examined. Section IV presents the design of decoupling controller to further increase system's performance. The stability and dynamic response are also analyzed. In Section V, both simulation and experimental results verify the analyses. In Section VI, several technical discussions are conducted for the proposed technique.

II. Average and Small Signal Models for CMI and Control to Output Transfer Function

A. Average and Small Signal Models

In Fig. 1(b), each multilevel inverter cell can generate three output voltage levels: –E, 0, E. To eliminate the dc component and the even order harmonics, it is common to synthesize the voltage waveform to be both odd and symmetric to $(2k-1)\pi/2, k=0,\pm1,\pm2,\pm3\ldots$ as shown in Fig. 1(b). Because the two switching angles of a cell are dependent, each cell only has one degree of freedom to control its output. The spectrum of the corresponding waveform in Fig. 1(b) can be expressed as

$$\begin{aligned} v_{cell\_n} = \ & \frac{4}{\pi}E\Big[\cos\theta_n\sin(\omega t)+\frac{1}{3}\cos 3\theta_n\sin(3\omega t) \\ & +\frac{1}{5}\cos 5\theta_n\sin(5\omega t)+\ldots\Big] \\ n = \ & 1,2,3. \end{aligned} \tag{1}$$

The overall output voltage is shown in Fig. 1(c) and its spectrum is given by

$$v_{out}=\frac{4}{\pi}E \begin{bmatrix} (\cos\theta_1+\cos\theta_2+\cos\theta_3)\sin(\omega t) \\ +\frac{1}{3}(\cos 3\theta_1+\cos 3\theta_2+\cos 3\theta_3)\sin(3\omega t) \\ +\frac{1}{5}(\cos 5\theta_1+\cos 5\theta_2+\cos 5\theta_3)\sin(5\omega t)+\ldots \end{bmatrix}. \tag{2}$$

As shown in (2), $v_{\rm out}$ has three degrees of freedom θ_1, θ_2 and θ_3. For a single-phase system, to eliminate third and fifth order harmonics, equation set (3) should be satisfied.

$$\begin{cases} v_{h1}=\frac{4}{\pi}(\cos\theta_1+\cos\theta_2+\cos\theta_3)E=V_{ref} \\ v_{h3}=\frac{4}{3\pi}(\cos 3\theta_1+\cos 3\theta_2+\cos 3\theta_3)E=0 \\ v_{h5}=\frac{4}{5\pi}(\cos 5\theta_1+\cos 5\theta_2+\cos 5\theta_3)E=0. \end{cases} \tag{3}$$

In (3), switching angle $\theta_n, n=1,2,3$ are control parameters and $v_{hi}, i=1,3,5$, the magnitudes of fundamental, third and fifth order harmonics are the output parameters. As shown in (3), all of these control and output parameters are coupled. $V_{\rm ref}$ is the reference voltage of fundamental. If modulation index m_{hi} is defined as $m_{hi}=v_{hi}/(4E/\pi), i=1,2,3$, applying the complete solution method introduced in [6], [7], [13], [14], [15], the equation set only has steady-state solutions in two modulation ranges, m_{h1} from 1.648 to 2.070, and m_{h1} from 2.407 to 2.456. In the ranges where the system has no solutions, the typical way is to keep the higher order harmonics uncontrolled [6], [7], [13], [14], [15], or keep the THD as low as possible. Because this paper focuses on developing precise solutions for transcendental equations, the range $m_{h1}\in[1.65, 2.00]$ is taken as an example and to be investigated in detail. Both simulations and experimental results are to be presented. The same analysis can also be applied to range [2.407, 2.456]. However, the range [2.407, 2.456] has a very limited adjustable voltage range of 0.16%, so it is mostly not used in practical cases. For the applicable ranges outside of [1.65, 2.00] and [2.407, 2.456], the same method can be applied and simulation results will be presented.

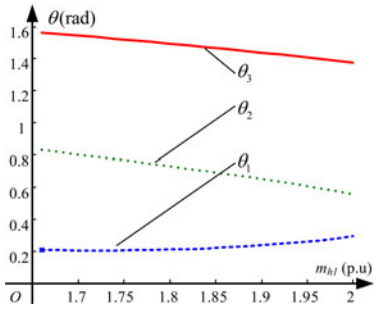

Fig. 2. Solutions of θ_1, θ_2 and θ_3 within $m_{h1} \in$[1.65, 2.00].

It should be pointed out that in (3), depending on the applications of the CMI, dc bus voltage E could be from different sources. It could be from the sources such as a bidirectional dc/dc converter or a battery which has relatively constant output voltages. On the other hand, it could be also from the sources such as a dc bus capacitor which has the second order voltage harmonic superposed. For the second case, harmonic suppression technique [19] should be employed otherwise using constant E may introduce some errors.

The steady-state solutions are shown in Fig. 2 for the modulation range $m_{h1} \in$ [1.65, 2.00]. The small signal modeling is presented in (4)

$$\begin{cases} v_{h1} = V_{h10} + \hat{v}_{h1} = \dfrac{4E}{\pi} \\ \left[\cos\left(\theta_{10}+\hat{\theta}_1\right) + \cos\left(\theta_{20}+\hat{\theta}_2\right) + \cos\left(\theta_{30}+\hat{\theta}_3\right)\right] \\ v_{h1} = V_{h10} + \hat{v}_{h1} = \dfrac{4E}{3\pi} \\ \left[\cos\left(\theta_{10}+\hat{\theta}_1\right) + \cos\left(\theta_{20}+\hat{\theta}_2\right) + \cos\left(\theta_{30}+\hat{\theta}_3\right)\right] \\ v_{h5} = V_{h50} + \hat{v}_{h5} = \dfrac{4E}{5\pi} \\ \left[\cos 5\left(\theta_{10}+\hat{\theta}_1\right) + \cos 5\left(\theta_{20}+\hat{\theta}_2\right) + \cos 5\left(\theta_{30}+\hat{\theta}_3\right)\right]. \end{cases} \tag{4}$$

In (4), $\theta_{10}, \theta_{20}, \theta_{30}$ are steady-state switching angles for cell 1, 2 and 3; $V_{h10}, V_{h30}, V_{h50}$ are steady-state amplitudes of first, third and fifth harmonics;$\hat{\theta}_1$,$\hat{\theta}_2$,$\hat{\theta}_3$ are switching angle perturbations for cell 1, 2 and 3; $\hat{v}_{h1}$,$\hat{v}_{h3}$,$\hat{v}_{h5}$ are amplitude perturbations of first, third and fifth harmonics. The first term on the right of the first equation can be expressed as

$$\begin{aligned} \cos(\theta_{10}+\hat{\theta}_1) &= \cos(\theta_{10})\cos(\hat{\theta}_1) - \sin(\theta_{10})sin(\hat{\theta}_1) \\ &= \cos(\theta_{10})\left(1 - \frac{1}{2}\hat{\theta}_1^2 + \frac{1}{4!}\hat{\theta}_1^4 + O(\hat{\theta}_1^4)\right) \\ &\quad -\sin(\theta_{10})\left(\hat{\theta}_1 - \frac{1}{3!}\hat{\theta}_1^3 + \frac{1}{5!}\hat{\theta}_1^5 + O(\hat{\theta}_1^5)\right) \\ &= \underbrace{\cos(\theta_{10})}_{\text{DC COMPONENT}} \quad \underbrace{-\sin(\theta_{10})\hat{\theta}_1 + O(\hat{\theta}_1)}_{\text{AC COMPONENT}}. \end{aligned} \tag{5}$$

Similarly, for the other terms in (4)

$$\begin{cases} \cos(\theta_{10}+\hat{\theta}_1) = \cos(\theta_{10}) - \sin(\theta_{10})\hat{\theta}_1 + O(\hat{\theta}_1) \\ \cos(3(\theta_{10}+\hat{\theta}_1)) = \cos(3\theta_{10}) - 3\sin(3\theta_{10})\hat{\theta}_1 + O(\hat{\theta}_1) \\ \cos(5(\theta_{10}+\hat{\theta}_1)) = \cos(5\theta_{10}) - 5\sin(5\theta_{10})\hat{\theta}_1 + O(\hat{\theta}_1). \end{cases} \tag{6}$$

(4) can therefore be decomposed to ac components and dc components. The average model and the small signal model are therefore given by (7) and (8), respectively

$$\begin{cases} V_{h10} = \dfrac{4E}{\pi}(\cos(\theta_{10}) + \cos(\theta_{20}) + \cos(\theta_{30})) \\ V_{h30} = \dfrac{4E}{3\pi}(\cos 3(\theta_{10}) + \cos 3(\theta_{20}) + \cos 3(\theta_{30})) \\ V_{h50} = \dfrac{4E}{5\pi}(\cos 5(\theta_{10}) + \cos 5(\theta_{20}) + \cos 5(\theta_{30})) \end{cases} \tag{7}$$

$$\begin{cases} \hat{v}_{h1} = -\dfrac{4E}{\pi}(sin(\theta_{10})\hat{\theta}_1 + sin(\theta_{20})\hat{\theta}_2 + sin(\theta_{30})\hat{\theta}_3) \\ \hat{v}_{h3} = -\dfrac{4E}{\pi}(sin(3\theta_{10})\hat{\theta}_1 + sin(3\theta_{20})\hat{\theta}_2 + sin(3\theta_{30})\hat{\theta}_3) \\ \hat{v}_{h5} = -\dfrac{4E}{\pi}(sin(5\theta_{10})\hat{\theta}_1 + sin(5\theta_{20})\hat{\theta}_2 + sin(5\theta_{30})\hat{\theta}_3). \end{cases} \tag{8}$$

(8) can be further expressed as

$$\begin{bmatrix} \hat{v}_{h1} \\ \hat{v}_{h3} \\ \hat{v}_{h5} \end{bmatrix} = -\frac{4E}{\pi}\begin{bmatrix} \sin\theta_{10} & \sin\theta_{20} & \sin\theta_{30} \\ \sin 3\theta_{10} & \sin 3\theta_{20} & \sin 3\theta_{30} \\ \sin 5\theta_{10} & \sin 5\theta_{20} & \sin 5\theta_{30} \end{bmatrix}\begin{bmatrix} \hat{\theta}_1 \\ \hat{\theta}_2 \\ \hat{\theta}_3 \end{bmatrix}. \tag{9}$$

The control to output transfer function $G_{v\theta}$ is defined by

$$\hat{v}_h = -\frac{4E}{\pi}T_1\hat{\theta} = G_{v\theta}\hat{\theta} \tag{10}$$

where

$$\hat{v}_h = \begin{bmatrix} \hat{v}_{h1} \\ \hat{v}_{h3} \\ \hat{v}_{h5} \end{bmatrix},\ \hat{\theta} = \begin{bmatrix} \hat{\theta}_1 \\ \hat{\theta}_2 \\ \hat{\theta}_3 \end{bmatrix},$$

$$T_1 = \begin{bmatrix} \sin\theta_{10} & \sin\theta_{20} & \sin\theta_{30} \\ \sin 3\theta_{10} & \sin 3\theta_{20} & \sin 3\theta_{30} \\ \sin 5\theta_{10} & \sin 5\theta_{20} & \sin 5\theta_{30} \end{bmatrix},\ G_{v\theta} = -\frac{4E}{\pi}T_1.$$

B. Discussion on Average and Small Signal Models

Average model and small signal model can be used in the modeling and control of CMI. It should be noted that in (5), it is assumed that $\hat{\theta}_1$ is small enough and $O(\hat{\theta}_1)$ can be eliminated. This assumption does not hold when $sin(\theta_{10})$ is close to zero. As an example, when $sin(\theta_{10})$ equals zero, no matter how small $\hat{\theta}_1$ is, this assumption is not met. Because of this, in some θ_n regions, ignoring $O(\hat{\theta}_n)$ may generate undesired errors. The errors must be evaluated before the small signal model can be used for dynamic response analysis. In this paper, Lyapunov's indirect method [10], [11] is used to determine system's stability

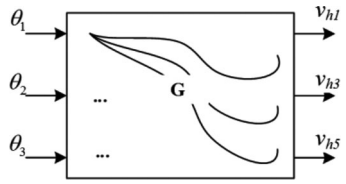

Fig. 3. Diagram of the controlled system.

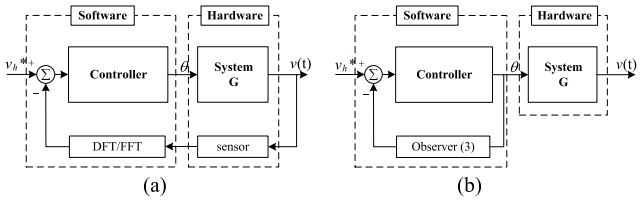

Fig. 4. Control diagram: (a) with DFT/FFT and (b) with an inner observer.

with the original system model from (3). Dynamic response will still be analyzed using the small signal model and the introduced errors due to the small signal model are evaluated and quantified. The small signal model is also useful to provide a concise and intuitive solution to evaluate the system's performance without strict mathematic proof.

III. Proposed Feedback Loop With Integral Controllers and a Transient-Free Inner Observer

A. Proposed Feedback Loop

This paper reconstructs the equation set (3) to be a controlled system G in Fig. 3. There are three inputs θ_1, θ_2 and θ_3 and three outputs v_{h1}, v_{h3}, v_{h5} in the diagram. The curves in this block represent nonlinear and coupling characteristics of the system rather than the actual relationships between the inputs and outputs.

The system G in Fig. 3 has following characteristics:

1) the multiple inputs and multiple outputs are coupled;
2) there is no time delay element exisiting in the block, or the system is memoryless;
3) the steady-state input θ_n is a dc value and can be represented with a step function;
4) caculating v_{hi} from θ_n is much easier than caculating θ_k from v_{hi}.

Because the reference input is a step function, an integral controller with unit gain can be used to achieve zero steady-state error. Fig. 4(a) shows a conventional feedback control diagram. Output voltage *v(t)* is sensed and the spectrum of *v(t)*is extracted with DFT/FFT. The spectrum is then compared with harmonic reference v_h^* to generate an error signal. The error signal is fed to an integral controller to generate switching angle θ. The switching angle θ is used to control the CMI. Significant phase delay is introduced by DFT/FFT; as a result, the system response is slow and may have stability issues. In Fig. 4(b), an instantaneous inner observer is proposed to extract the spectrum of *v(t)* from the switching angle θ based on equation (3) without phase delay.

The detail control diagram of the system with a LUT, integral controllers and a transient-free inner observer is shown in Fig. 5. In Fig. 5, a small LUT is employed in the feed-forward path to provide initial θ to achieve fast dynamic response and ensure that the system is so close to a steady state that small signal model can be applied during dynamic response analysis. Three unit-gain integral controllers are employed to compensate the error between the initial θ and the accurate θ to finally achieve zero steady-state error.

In Fig. 5, the system's transfer equation can be expressed as

$$\begin{cases} \dot{\hat{\theta}}_1 = K_1(v_{h1}^* - v_{h1}) \\ \dot{\hat{\theta}}_2 = K_2(v_{h3}^* - v_{h3}) \\ \dot{\hat{\theta}}_3 = K_3(v_{h5}^* - v_{h5}) \end{cases}$$

where v_{h1}, v_{h3} and v_{h5} are given by (4) or

$$\begin{cases} \dot{\hat{\theta}}_1 = K_1 \Big(v_{h1}^* - \frac{4E}{\pi}(\cos(\theta_{10} + \hat{\theta}_1) + \cos(\theta_{20} + \hat{\theta}_2) \\ \qquad + \cos(\theta_{30} + \hat{\theta}_3)) \Big) \\ \dot{\hat{\theta}}_2 = K_2 \Big(v_{h3}^* - \frac{4E}{3\pi}(\cos 3(\theta_{10} + \hat{\theta}_1) + \cos 3(\theta_{20} + \hat{\theta}_2) \\ \qquad + \cos 3(\theta_{30} + \hat{\theta}_3)) \Big) \\ \dot{\hat{\theta}}_3 = K_3 \Big(v_{h5}^* - \frac{4E}{5\pi}(\cos 5(\theta_{10} + \hat{\theta}_1) + \cos 5(\theta_{20} + \hat{\theta}_2) \\ \qquad + \cos 5(\theta_{30} + \hat{\theta}_3)) \Big). \end{cases} \tag{11}$$

It is assumed that at equilibrium state, $\left[\hat{\theta}_1, \hat{\theta}_2, \hat{\theta}_3\right]^T = [z_1, z_2, z_3]^T = \mathrm{z}$, where $\hat{\theta}_1, \hat{\theta}_2, \hat{\theta}_3 \in [-\lim, \lim]$. The limits guarantee the system is within stable region and will be discussed later. They can be implemented with the integral blocks in Fig. 5.

B. Stability Analysis With Lyapunov's Indirect Method

As indicated previously, small signal model cannot be used to analyze system's stability because small signal assumption is not met in some θ_n regions. However, based on nonlinear control theory, the indirect method of Lyapunov [10], [11] can be used to determine system's stability. The Jacobian matrix used for stability analysis is derived directly from (11) as

$$A|_{\hat{\theta}=z} = \left.\frac{\partial \dot{\hat{\theta}}}{\partial \hat{\theta}}\right|_{\hat{\theta}=z} = \frac{4E}{\pi} \begin{bmatrix} K_1 \sin(\theta_{10} + z_1) & K_1 \sin(\theta_{20} + z_2) \\ K_1 \sin(\theta_{30} + z_3) & \\ K_2 \sin(3(\theta_{10} + z_1)) & K_2 \sin(3(\theta_{20} + z_2)) \\ K_2 \sin(3(\theta_{30} + z_3)) & \\ K_3 \sin(5(\theta_{10} + z_1)) & K_3 \sin(5(\theta_{20} + z_2)) \\ K_3 \sin(5(\theta_{30} + z_3)) & \end{bmatrix}. \tag{12}$$

If the eigenvalues of *A* is λ_1, λ_2 and λ_3, based on the indirect the method of Lyapunov, if $Re(\lambda_i) < 0, i = 1, 2, 3$, the system

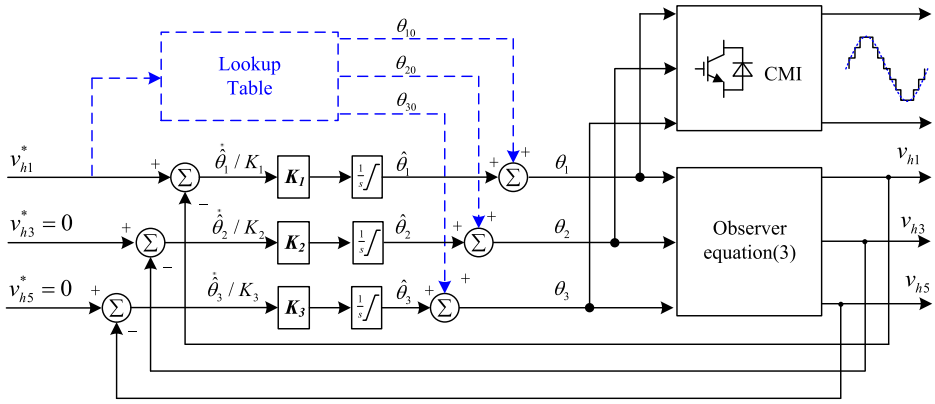

Fig. 5. System control block diagram with a LUT, integral controllers and a transient-free inner observer.

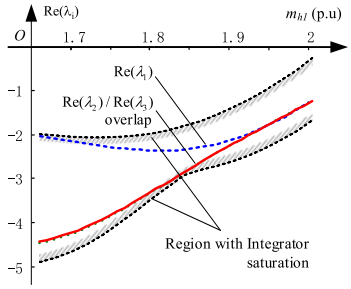

Fig. 6. Trajectories of $Re(\lambda_i), m_{h1} \in$[1.65,2.00].

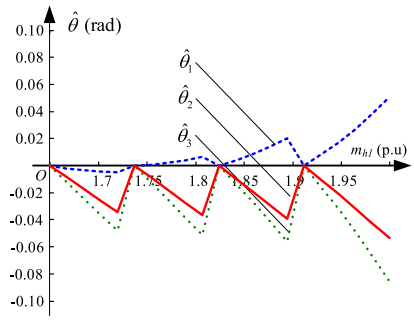

Fig. 7. Steady-state $\hat{\theta}_1, \hat{\theta}_2, \hat{\theta}_3$ are within the limits.

is stable. The trajectories of $Re(\lambda_i)$ when $K_1 = 10, K_2 = -1$ and $K_3 = -10$ is shown in Fig. 6. All of them are below zero in the modulation range $m_{h1} \in [1.65, 2.00]$, so the system is stable for given K_1, K_2 and K_3. It should be pointed out that because the relationship between inputs $\theta_1, \theta_2, \theta_3$, and outputs v_{h1}, v_{h3}, v_{h5} can be either positive or negative and they are coupled in the controlled system, the controller's proportional coefficient K_1, K_2 and K_3 could be either positive/negative to meet the stability requirement.

In a real application, if the reference $m_{h1}*$ has a sudden changes, $\hat{\theta}$ has a large variation from steady-state z. The system may enter an unstable region. Therefore, the range of $\hat{\theta}_n$ must be limited. The limits of $\hat{\theta}_n$ are set by the three integration blocks to ensure $Re(\lambda_i) < 0$, so the system stays within the stable region during any dynamic responses. Fig. 6 also shows the region with three integrators are limited at $[-0.1, 0.05]$, $[-0.05, 0.01]$ and $[-0.08, 0.01]$, respectively. $Re(\lambda_i) <$ is always within the region and the region is below zero; so the system is always stable. On the other hand, the limits of $\hat{\theta}_n$ should be larger than the maximum $\hat{\theta}_n$ during steady state so it would not affect steady-state operation. The steady-state $\hat{\theta}_n$ when m_{h1} varies from 1.65 to 2.0 are shown in Fig. 7. They are within the limits so the limits do not affect steady-state operation.

IV. Decoupling Controller and Dynamic Response Analysis With Small Signal Model

A. Decoupling Controller

The feedback loop with integral controller and transient-free inner observer discussed in Section III are used to control the system to reach a steady state. However, K_1, K_2 and K_3 are complicated to design because all the inputs $\hat{\theta}_n$ and outputs v_{hi} are coupled. The effects of K_1, K_2 and K_3 on the stability and dynamic response of the system is not straightforward. It is necessary to insert a decoupling controller to decouple them.

From the small signal model in (10), the decoupling controller can be designed as

$$\hat{\theta} = -\frac{\pi}{4E} T_l^{-1} \hat{v}_h \tag{13}$$

where T_l is the matrix defined in (10).

The inserted decoupling controller transforms the original coupled system to three separate unit blocks as shown later in Fig. 10; the relationship between the PI controller and system's steady state and dynamic response is therefore easy to analyze and it benefits the controller's parameter design.

The system's control diagram with the decoupling controller is shown in Fig. 8. To avoid calculating matrix inverse, T_l^{-1} instead T_l is stored in the LUT, and its resolution is the same as θ. The state variables of the system are $[\dot{v}_{h1}, \dot{v}_{h3}, \dot{v}_{h5}]$. The state space equations of the system are

$$\begin{cases} \dot{\hat{v}}_{h1} = K_1(v_{h1}^* - v_{h1}) \\ \dot{\hat{v}}_{h3} = K_2(v_{h3}^* - v_{h3}) \\ \dot{\hat{v}}_{h5} = K_3(v_{h5}^* - v_{h5}) \end{cases} \tag{14}$$

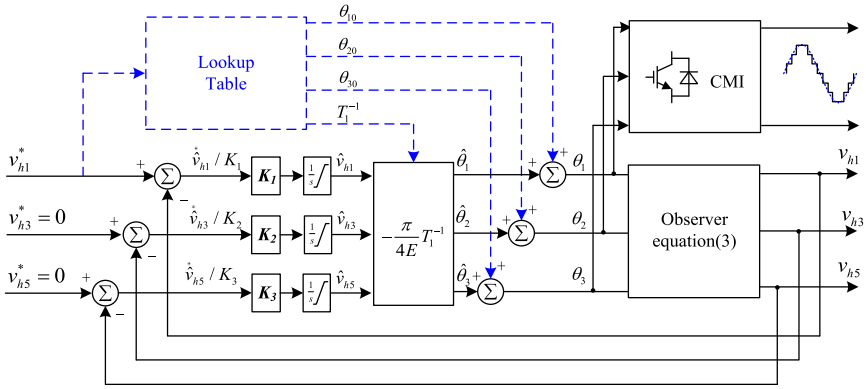

Fig. 8. System control block diagram with a LUT, integral controllers and a transient-free inner observer.

or

$$\begin{bmatrix}\dot{\hat{v}}_{h1}\\ \dot{\hat{v}}_{h3}\\ \dot{\hat{v}}_{h5}\end{bmatrix}=\begin{bmatrix}K_1&0&0\\0&K_2&0\\0&0&K_3\end{bmatrix}\left(\begin{bmatrix}v_{h1}^*\\v_{h3}^*\\v_{h5}^*\end{bmatrix}-\begin{bmatrix}v_{h1}\\v_{h3}\\v_{h5}\end{bmatrix}\right) \tag{15}$$

or $\dot{\hat{v}}_h = K\,(v_h^* - v_h)$where, $v_{\rm hi}$ is the amplitude of fundamental and harmonics; $v_{\rm hi}{}^*$ is the amplitude reference of fundamental and harmonics; $\dot{\hat{v}}_{hi}$ is the state variables of the systems; and

$$\dot{\hat{v}}_h=\begin{bmatrix}\dot{\hat{v}}_{h1}\\ \dot{\hat{v}}_{h3}\\ \dot{\hat{v}}_{h5}\end{bmatrix},K=\begin{bmatrix}K_1&0&0\\0&K_2&0\\0&0&K_3\end{bmatrix},v_h^*=\begin{bmatrix}v_{h1}^*\\v_{h3}^*\\v_{h5}^*\end{bmatrix},v_h=\begin{bmatrix}v_{h1}\\v_{h3}\\v_{h5}\end{bmatrix}.$$

B. Evaluate the Errors Introduced by Small Signal Model

To evaluate the errors introduced by ignoring the second order terms in (9), (6) is rewritten to (16) with $\hat{\theta}^2$ retained

$$\begin{cases}\cos(\theta_{10}+\hat{\theta}_1)=\cos(\theta_{10})-\sin(\theta_{10})\hat{\theta}_1\\ \quad-\cos(\theta_{10})\frac{1}{2}\hat{\theta}_1^2+O(\hat{\theta}_1^2)\\ \cos(3(\theta_{10}+\hat{\theta}_1))=\cos(3\theta_{10})-3\sin(3\theta_{10})\hat{\theta}_1\\ \quad-\cos(3\theta_{10})\frac{9}{2}\hat{\theta}_1^2+O(\hat{\theta}_1^2)\\ \cos(5(\theta_{10}+\hat{\theta}_1))=\cos(5\theta_{10})-5\sin(5\theta_{10})\hat{\theta}_1\\ \quad-\cos(5\theta_{10})\frac{25}{2}\hat{\theta}_1^2+O(\hat{\theta}_1^2).\end{cases} \tag{16}$$

Because the coefficients of $\hat{\theta}$ and $\hat{\theta}^2$ are orthogonal and they cannot be zero at the same time, the dominant component in ac components is always retained; so this model would be accurate enough to evaluate the system's dynamic response.

Substituting (4), (7), (13), (16) to (15) yields

$$\begin{bmatrix}\dot{\hat{v}}_{h1}\\ \dot{\hat{v}}_{h3}\\ \dot{\hat{v}}_{h5}\end{bmatrix}=\begin{bmatrix}K_1&0&0\\0&K_2&0\\0&0&K_3\end{bmatrix}\left(\begin{bmatrix}v_{h1}^*\\v_{h3}^*\\v_{h5}^*\end{bmatrix}-\begin{bmatrix}V_{h10}\\V_{h30}\\V_{h50}\end{bmatrix}\right)$$

$$+\frac{4}{\pi}ET_1\begin{bmatrix}\hat{\theta}_1\\ \hat{\theta}_2\\ \hat{\theta}_3\end{bmatrix}+$$

$$\frac{2}{\pi}E\begin{bmatrix}\cos(\theta_{10})&\cos(\theta_{20})&\cos(\theta_{30})\\3\cos(3\theta_{10})&3\cos(3\theta_{20})&3\cos(3\theta_{30})\\5\cos(5\theta_{10})&5\cos(5\theta_{20})&5\cos(5\theta_{30})\end{bmatrix}\begin{bmatrix}\hat{\theta}_1^2\\ \hat{\theta}_2^2\\ \hat{\theta}_3^2\end{bmatrix}\Bigg)$$

$$=\begin{bmatrix}K_1&0&0\\0&K_2&0\\0&0&K_3\end{bmatrix}\left(\begin{bmatrix}v_{h1}^*\\v_{h3}^*\\v_{h5}^*\end{bmatrix}-\begin{bmatrix}V_{h10}\\V_{h30}\\V_{h50}\end{bmatrix}-\begin{bmatrix}\hat{v}_{h1}\\ \hat{v}_{h3}\\ \hat{v}_{h5}\end{bmatrix}+\right.$$

$$\left.\frac{2}{\pi}E\begin{bmatrix}\cos(\theta_{10})&\cos(\theta_{20})&\cos(\theta_{30})\\3\cos(3\theta_{10})&3\cos(3\theta_{20})&3\cos(3\theta_{30})\\5\cos(5\theta_{10})&5\cos(5\theta_{20})&5\cos(5\theta_{30})\end{bmatrix}\begin{bmatrix}\hat{\theta}_1^2\\ \hat{\theta}_2^2\\ \hat{\theta}_3^2\end{bmatrix}\right). \tag{17}$$

If

$$\mathrm{ERR}=\frac{2}{\pi}E\begin{bmatrix}\cos(\theta_{10})&\cos(\theta_{20})&\cos(\theta_{30})\\3\cos(3\theta_{10})&3\cos(3\theta_{20})&3\cos(3\theta_{30})\\5\cos(5\theta_{10})&5\cos(5\theta_{20})&5\cos(5\theta_{30})\end{bmatrix}\begin{bmatrix}\hat{\theta}_1^2\\ \hat{\theta}_2^2\\ \hat{\theta}_3^2\end{bmatrix} \tag{18}$$

then

$$\begin{bmatrix}\dot{\hat{v}}_{h1}\\ \dot{\hat{v}}_{h3}\\ \dot{\hat{v}}_{h5}\end{bmatrix}=\begin{bmatrix}K_1&0&0\\0&K_2&0\\0&0&K_3\end{bmatrix}$$

$$\left\{\underbrace{\begin{bmatrix}v_{h1}^*\\v_{h3}^*\\v_{h5}^*\end{bmatrix}-\begin{bmatrix}V_{h10}\\V_{h30}\\V_{h50}\end{bmatrix}}_{\text{input}}-\underbrace{\begin{bmatrix}\hat{v}_{h1}\\ \hat{v}_{h3}\\ \hat{v}_{h5}\end{bmatrix}}_{\text{state}}+\mathrm{ERR}\right\}. \tag{19}$$

ERR represents the error introduced by (9) due to the fact that the second order terms are ignored. Because of the limits added to integral controller, ERR is bounded. Fig. 9(a) shows

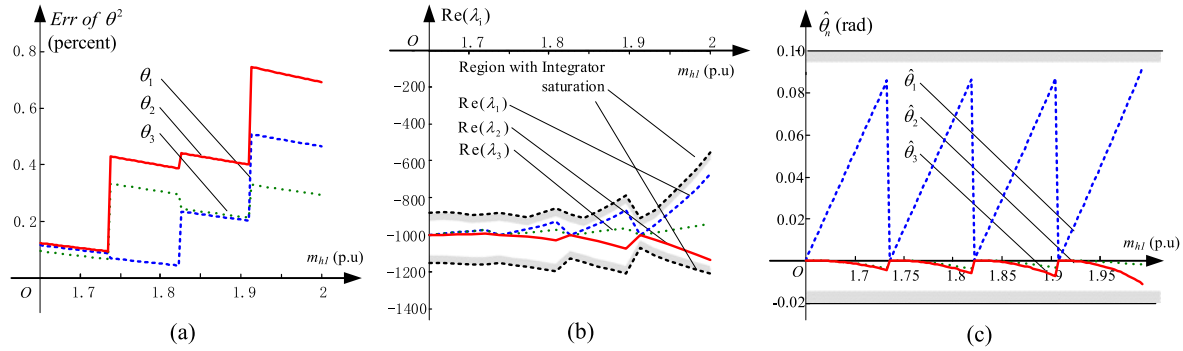

Fig. 9. Characteristics of the decoupled system. (a) Error introduced by ignoring θ^2. (b) Trajectories of $Re(\lambda_i)$. (c) Determine the limits for integral controllers.

the introduced ERR is less than 2%, so the developed model based on the first order approximation is valid.

C. System Stability With Decoupling Controller

Similar to Section III, it is assumed that at a steady state, $\hat{v}_h = v_z$ and $\hat{\theta} = z$. The Jacobian matrix which determines the system's stability is found from (4), (13) and (15) as equation (20) as shown at the bottom of the page.

Fig. 9(b) shows the trajectories of the real part of the eigenvalues when $K_1 = K_2 = K_3 = 1000$. As analyzed previously, the outputs of integral controllers should be limited to guarantee the system is in stable region during dynamic responses. Fig. 9(b) also shows the region with three integrators are limited at $[-0.02, 0.10]$, $[-0.01, 0.01]$ and $[-0.01, 0.01]$, respectively. In Fig. 9(b), $Re(\lambda_i)$ is within the limited region and the region is below zero; so the system is always stable. As analyzed previously, the limits should be larger than the maximum $\hat{\theta}_n$ during steady state so it would not affect steady-state operation. The steady-state $\hat{\theta}_n$ when m_{h1} varies from 1.65 to 2.0 is shown in Fig. 9(c). All $\hat{\theta}_n$ are within their limits so the limits do not affect steady-state operation.

D. Analysis of Dynamic Response Using Small Signal Model

Fig. 10 shows that the functions of decoupling matrix, LUT and the observer are equivalent to a block. In the block, the initial values of fundamental and harmonics are determined by V_{h0} which is equivalently determined by LUT. The inner close feedback loop equivalently regulates the $\hat{v}_h$ to finally reach a zero-error steady state. The gain of the decoupling controller, LUT and the observer can be represented with a unit gain block in the figure.

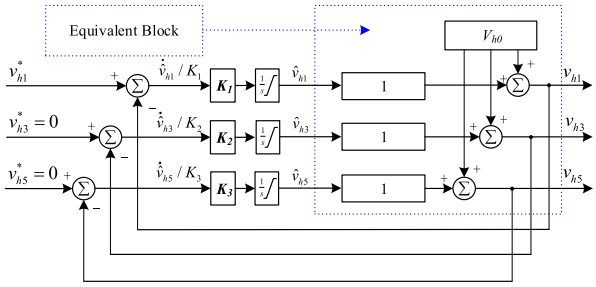

Fig. 10. Equivalent circuit with the decoupling controller.

Based on (19) and Fig. 10, the system is composed of three separate first order systems. The time constants of these three systems are $1/K_1, 1/K_2$ and $1/K_3$. If reference v_h* changes from V_1 to V_2, the dynamic response of the system is represented as

$$\Delta\hat{v}_h(t) = [(V_2 - V_{20}) - (V_1 - V_{10})]\left(1 - e^{-Kt}\right). \quad (21)$$

In (21), V_{10} and V_{20} are initial values from LUT. $\Delta\hat{v}_h(t)$ is the difference between the final steady-state value and the output value. (21) shows that the initial deviation of the output voltage from the final steady-state value is decided by the difference between $(V_2 - V_{20})$ and $(V_1 - V_{10})$. The time constant is decided by K. Because K_1, K_2 and K_3 are real positive numbers, the system is always stable during the transient. In this case, $(V_2 - V_{20}) - (V_1 - V_{10}) \in \left[-0.0875\frac{4}{\pi}E,\ 0.0875\frac{4}{\pi}E\right]$. If K is large enough, the system can be settled down within one fundamental period.

V. Simulation and Experimental Results

Because the purpose of simulations and experiments is to test if the output voltage of a CMI performs as expected with

$$A|_{\hat{v}_h = v_z} = \left.\frac{\partial\dot{\hat{v}}_h}{\partial\hat{v}_h}\right|_{\hat{v}_h = v_z} = \left.\frac{\partial\dot{\hat{v}}_h}{\partial\hat{\theta}}\frac{\partial\hat{\theta}}{\partial\hat{v}_h}\right|_{\hat{v}_h = v_z} =$$

$$\begin{bmatrix} -K_1 & 0 & 0 \\ 0 & -K_2 & 0 \\ 0 & 0 & -K_3 \end{bmatrix} T_1^{-1} \begin{bmatrix} \sin(\theta_{10} + z_1) & \sin(\theta_{20} + z_2) & \sin(\theta_{30} + z_2) \\ \sin(3(\theta_{10} + z_1)) & \sin(3(\theta_{20} + z_2)) & \sin(3(\theta_{30} + z_3)) \\ \sin(5(\theta_{10} + z_1)) & \sin(5(\theta_{20} + z_2)) & \sin(5(\theta_{30} + z_3)) \end{bmatrix} \quad (20)$$

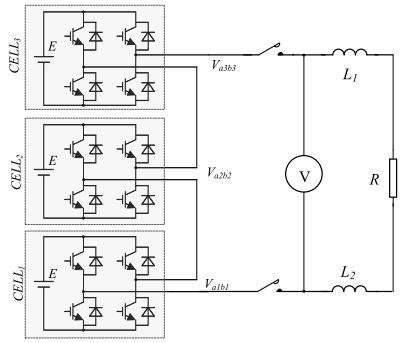

Fig. 11. Scale-down, 300-W, three-cell-CMI testbed.

TABLE I
PARAMETERS OF THE TEST SETUP

Dc bus voltage of each cell	50 V
Rated output voltage (peak)	127 V/60 Hz
Load inductance L_1	1 mH
Load inductance L_2	1 mH
Load resistance R	100 Ω
Sampling frequency	72 kHz
Switching frequency	60 Hz

the developed technique, a scale-down, 300-W, three-cell CMI with a *RL* load in Fig. 11 is enough for experiments. The parameters are listed in Table I. The dc bus voltage of each cell is 50 V. The algorithm was implemented with a TMS320F2812 fixed-point digital signal processor. Simulations were first performed using the power system module in MATLAB Simulink. In experiments, the time domain waveforms were recorded with Yokagawa ScopeCorder DLM2034 digital oscilloscope. FFT was conducted with the integrated Xviewer. Both simulations and experiments were implemented with the control scheme in Fig. 8. $K_1, K_2, K_3 = 1000$. The control flow is shown in Fig. 15. The interruption (INT) frequency is 72 kHz, which is also the discrete frequency of the control system. The reference m_{h1}^* and output angles are updated only once at the beginning of each fundamental period to prevent any undesired dc components during a transient. The 60-Hz period is implemented by the block, loop-by-1200-times, in this experiment. Based on (21), after one fundamental period 16.67 ms, $\Delta\hat{v}_h(t)$ is less than $0.1E \times 1e^{-16.67}$. Although a higher *K* can achieve faster dynamic response, the output angles are not updated until after a fundamental period; so the speed is limited by this. Furthermore, the algorithm is realized in a discrete digital system, a higher *K* requires a higher sampling frequency and a higher bandwidth. So if the dynamic response satisfies the requirement, *K* should be kept small. For this case, the desired setting time is 16.67 ms, sampling frequency is 1200 times than fundamental frequency, so $K_{1,2,3} = 1000$ is a good choice.

Figs. 12 and 13 show the simulated and experimentally measured results using the proposed technique. The reference is 110.7 V for the fundamental and zero for the third and fifth harmonics. The measured results match the simulated. The fundamental voltage is close to 110.7 V and the third and fifth harmonics are eliminated.

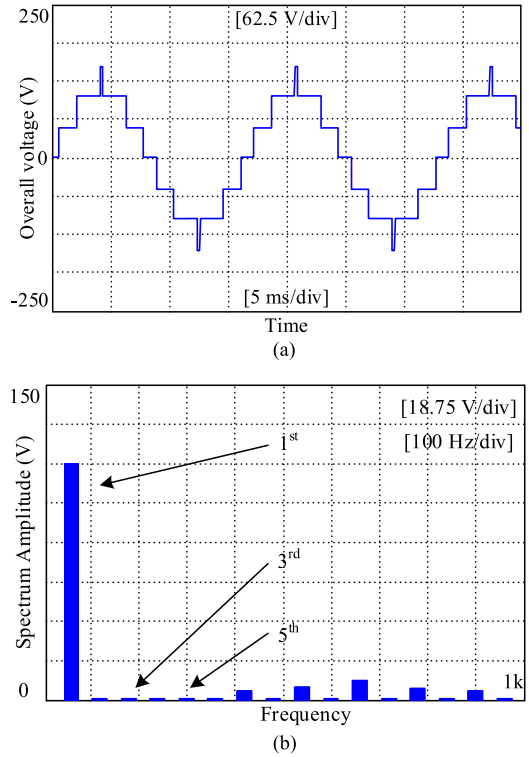

Fig. 12. Simulated steady-state results with fundamental reference as $v_{h1}^* = 110.7$ V, $v_{h3}^* = 0$ V, $v_{h5}^* = 0$ V, (a) overall voltage waveform and (b) FFT results of the voltage waveform.

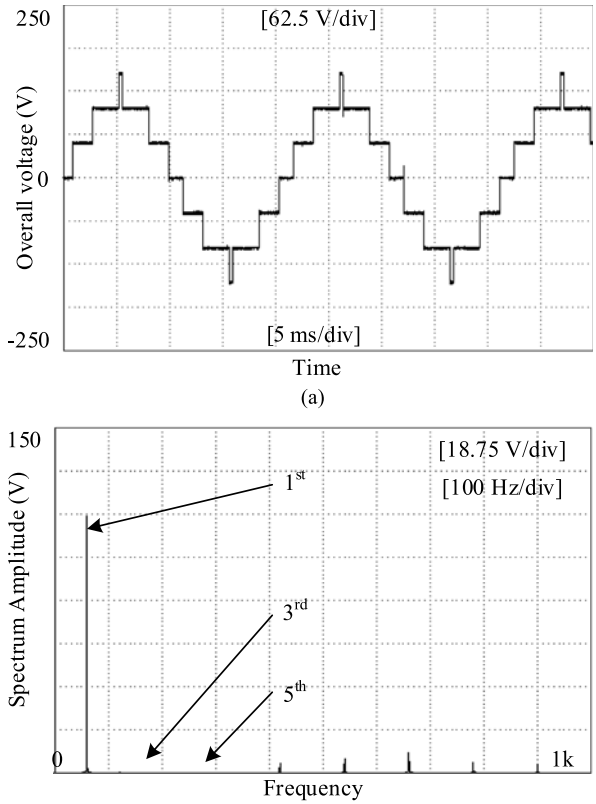

Fig. 13. Measured steady-state results with fundamental reference as $v_{h1}^* = 110.7$ V, $v_{h3}^* = 0$ V, $v_{h5}^* = 0$ V, (a) overall voltage waveform and (b) FFT results of the voltage waveform.

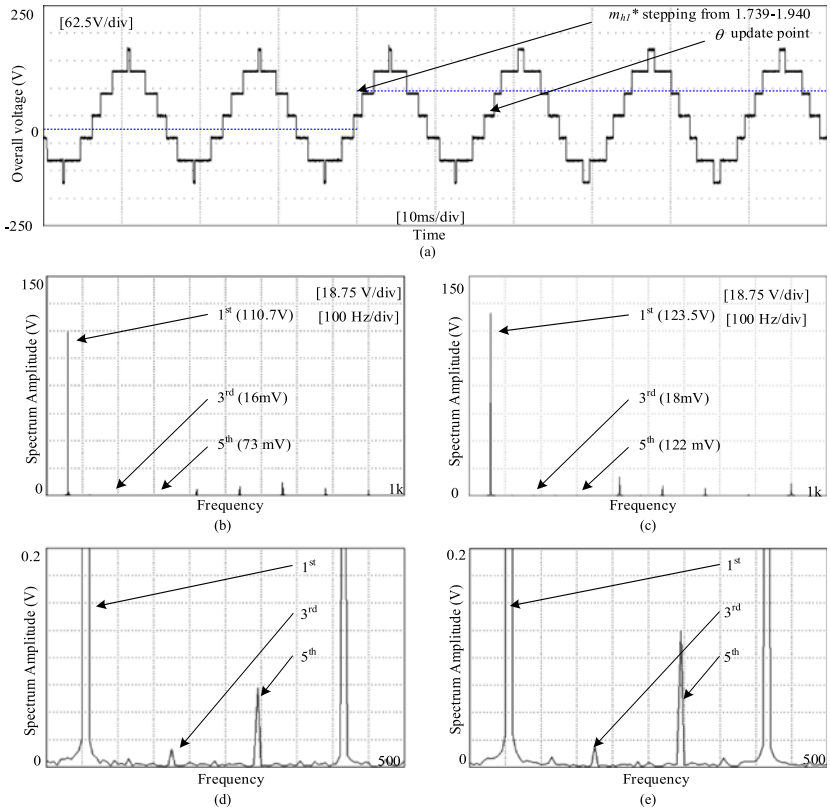

Fig. 14. Dynamic response of the system with m_{h1} stepping from $1.749 \sim 1.940$, (a) overall voltage waveform, (b) voltage spectrum with $m_{h1}^* = 1.739$, (c) voltage spectrum with $m_{h1}^* = 1.940$, (d) enlarged voltage spectrum with $m_{h1}^* = 1.739$, (e) enlarged voltage spectrum with $m_{h1}^* = 1.940$.

Fig. 14 shows the measured dynamic response of output voltage and spectrums using the proposed technique. The dotted line in Fig. 14(a) shows the fundamental reference m_{h1}^* changes from 1.739–1.940 which is correspondent to the fundamental voltage reference changes from 110.7 to 124 V. Fig. 14(a) also shows the measured voltage waveform. Fig. 14(b) and (c) are the FFT results before and after the reference changes separately. With the abrupt change of the fundamental reference, the switching angles of cells changed correspondently within no more than one fundamental period as shown in Fig. 14(a). The FFT result shows that the system has zero steady-state error in both before and after reference change. It verifies the advantages of transient-free and zero steady-state error by using the developed technique. Fig. 14(d) and (e) shows the enlarged, measured harmonic spectrum. It is shown that due to the proposed inner loop feedback, the third and fifth harmonics are almost totally eliminated.

Fig. 16 shows the dynamic response of error signals which is directly derived from the DSP chip. At the time the reference changes, the ERR of m_{h1} increases to more than 10%. The LUT feed-forward loop decreases the ERR to -4.5% quickly. The integral controller finally reaches a zero-error steady state within one fundamental period. During the dynamic response, due to the limited resolution of T_l^{-1} stored in LUT, m_{h3} increases by 0.24%, but is quickly suppressed by its own feedback loop. Because the system is essentially a first order system, no overshoot is observed. All the errors diminish to below 0.5% within 5 ms. This proves that the proposed algorithm can realize SHE within one fundamental period.

VI. Discussion

In this section, the proposed technique will be used to eliminate other orders of harmonics and it will be applied to the modulation ranges outside of [1.65, 2.0]. With a simple voltage feedback loop, the proposed technique can be applied to CMIs with varying dc bus voltages. The number of data points to be stored in LUT will be addressed in this section. The comparison of the number of data stored in LUTs between the proposed technique and the conventional technique will be presented. The technique to design the K_1, K_2 and K_3 in Fig. 8 will also be explored.

A. Applying the Developed Technique to Eliminate Other Order of Harmonics

As stated in Section I, the three-cell CMI can also be used to eliminate other order of harmonics such as fifth and seventh. Fig. 17(a) and (b) shows the simulated output voltage waveform and harmonic spectrum with fifth and seventh harmonics eliminated using the proposed technique in a three-cell CMI. The proposed technique in this paper can also be applied to the CMI with more number of cells to eliminate more orders of harmonics. Fig. 18(a) and (b) shows the simulated output voltage waveform and harmonic spectrum with third, fifth, seventh,

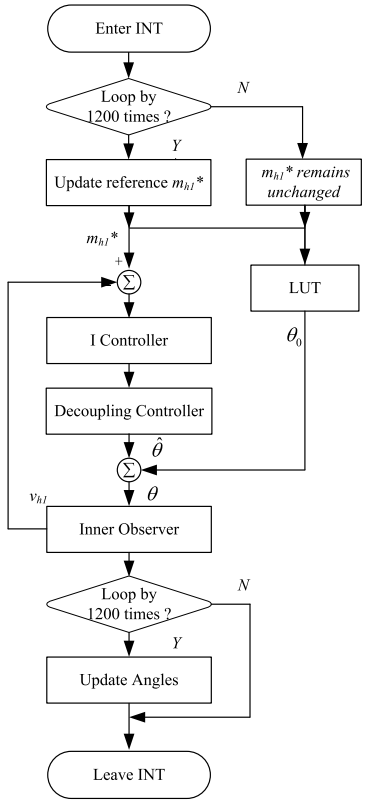

Fig. 15. Control flow chart of DSP.

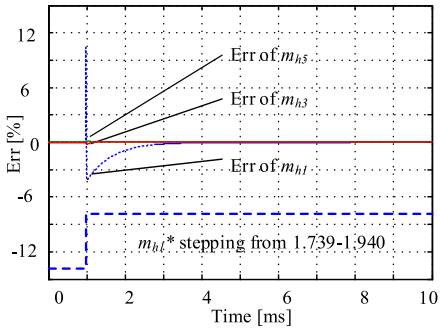

Fig. 16. Dynamic response of ERR with m_{h1} reference stepping from $1.739 \sim 1.940$.

ninth and eleventh harmonics eliminated using the proposed technique in a six-cell CMI.

B. Applying the Developed Technique to the Modulation Range Outside of [1.65, 2.0]

When the modulation index m is larger than 2.0, for a three-cell CMI, one cell is always in on state. One degree of control freedom is therefore lost [6], [7], [13], [14], so only one harmonic can be eliminated. For example, only the third harmonic is eliminated and the fundamental is maintained. The simulation results for $m = 2.51$ are shown in Fig. 19.

In the simulation, the system's reference modulation index m_{ref} is 2.51 and reference voltage V_{ref} is 160 V. The corresponding data stored in LUT have a modulation index of 2.0

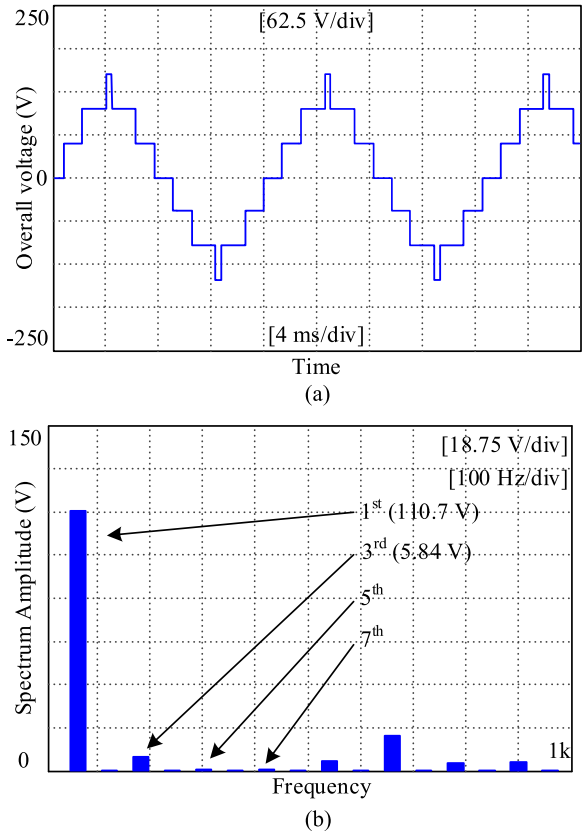

Fig. 17. Simulated steady-state results using the proposed technique in a three-cell CMI to eliminate fifth and seventh harmonics, (a) overall voltage waveform and (b) FFT result of the voltage waveform.

with a reference voltage 127.3 V. The errors between the references and the data stored in LUT are compensated by the proposed feedback controller.

When the modulation index m is smaller than 1.65, one cell is always in off (bypass) state. One degree of control freedom is lost. For example, only the third harmonic is eliminated and the fundamental is maintained. The simulation results for $m = 0.94$ are shown in Fig. 20.

In the simulation, the system's reference modulation index m_{ref} is 0.94 and reference voltage V_{ref} is 60 V. The corresponding data stored in LUT have a modulation index of 1.65 with a reference voltage 105 V. The errors between the references and the data stored in LUT are compensated by the proposed feedback controller.

C. Applying the Developed Technique to the CMI With Varying DC Bus Voltages

It is well known that in CMI, the power in each cell could be unbalanced. It leads to unbalanced dc bus voltage. Techniques such as first turn-on/first turn-off [12], rotating cell sequence [12], etc., can be used to balance the cell power and dc bus voltage. It should be pointed out that with an extra voltage *v(t)* feedback from the output to observer as shown in Fig. 21, the proposed feedback loop can regulate the switching angle of each cell to adapt the unbalanced voltage so it can still accurately

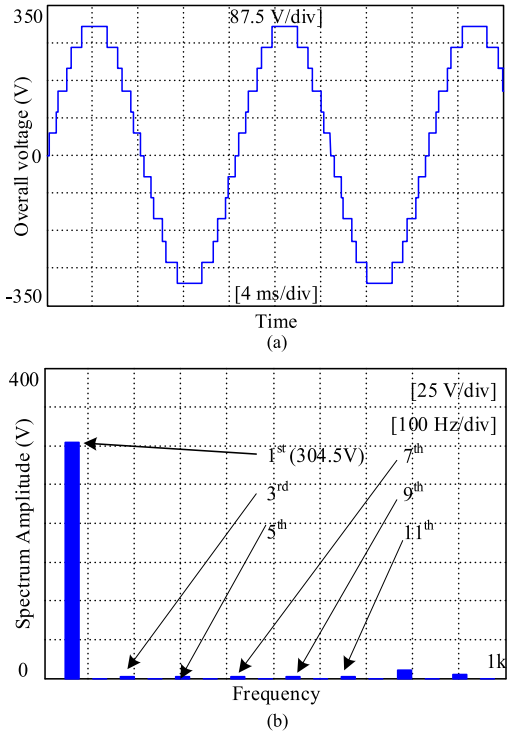

Fig. 18. Simulated steady-state results using the proposed technique in a six-cell CMI to eliminate third, fifth, seventh, ninth and eleventh harmonics, (a) overall voltage waveform and (b) FFT result of the voltage waveform.

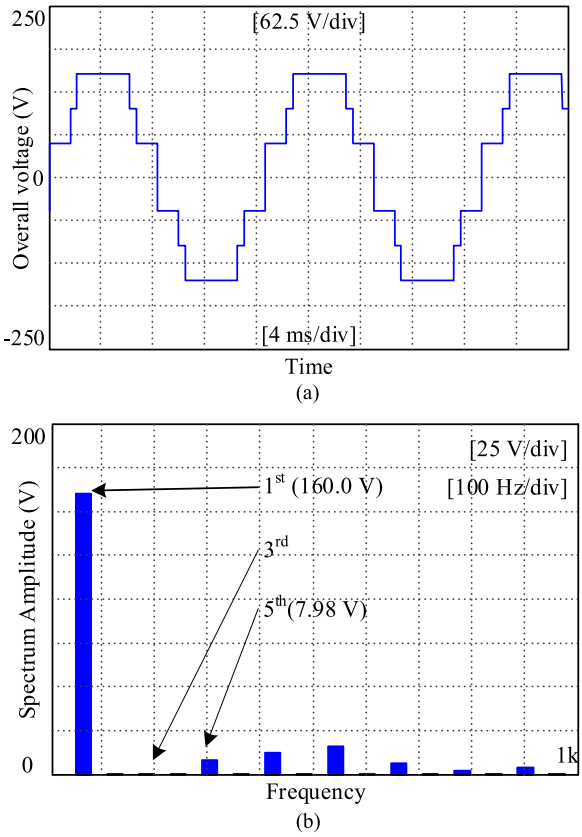

Fig. 19. Simulated steady-state results using the proposed technique in a three-cell CMI to eliminate third harmonic when $m = 2.51$, (a) overall voltage waveform and (b) FFT result of the voltage waveform.

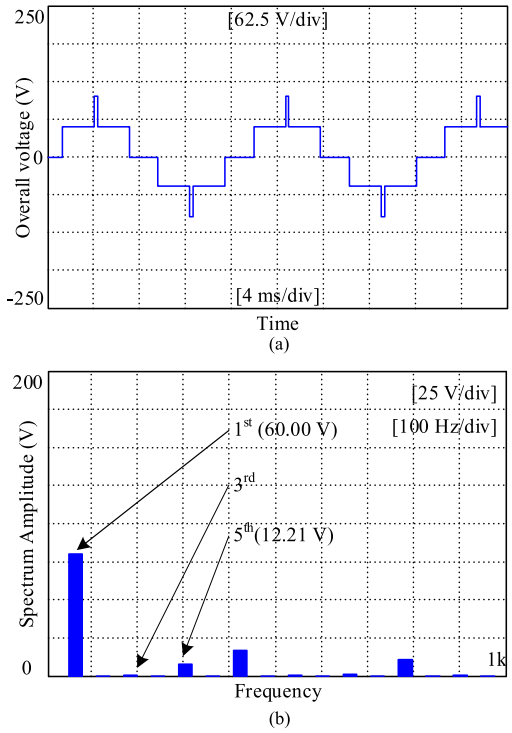

Fig. 20. Simulated steady-state results using the proposed technique in a three-cell CMI to eliminate third harmonic when $m = 0.94$, (a) overall voltage waveform and (b) FFT result of the voltage waveform.

achieve harmonic elimination. The magnitudes E_1, E_2 and E_3 of the output voltage of each cell can be easily sensed in time domain without doing FFT. The sensed output voltages are used to derive v_{h1}, v_{h3} and v_{h5} in (3). Fig. 22 and Table II show the simulated and measured voltage waveforms and harmonic spectrum with unbalanced voltages in a CMI using this voltage feedback.

In Table II, case 1 is with unbalanced dc voltage and without feedback control loop; case 2 is with balanced dc bus voltage; case 3 is with unbalanced dc voltage, voltage feedback and the proposed control loop; case 4 is experimental results. As shown from the simulation and experimental results in Table II and Fig. 22, with the proposed feedback loop, even with unbalanced dc bus voltage, the third and fifth harmonics can be successfully eliminated.

D. Design the Number of the Data Points Stored in LUT

In Fig. 9(c), with the decoupling matrix T_l^{-1}, the inputs $\hat{\theta}_i$ are proportional to Δm_{hj} which is the jth modulation index difference between the reference value and the value stored in the LUT. For third and fifth harmonics, both the modulation index for the reference and the value in LUT are zero, so $\hat{\theta}_2$ and $\hat{\theta}_3$ are almost zero; the blue dash line in Fig. 9(c) shows $\hat{\theta}_1$ as a function of m_{h1}. There are four segments in the range of [1.65, 2.0]. Within each segment, the line is linear with a slope of one. The peak value of each segment should be smaller than the saturation limits defined by the two lines on the top and bottom. Due to their linear characteristics, four segments should

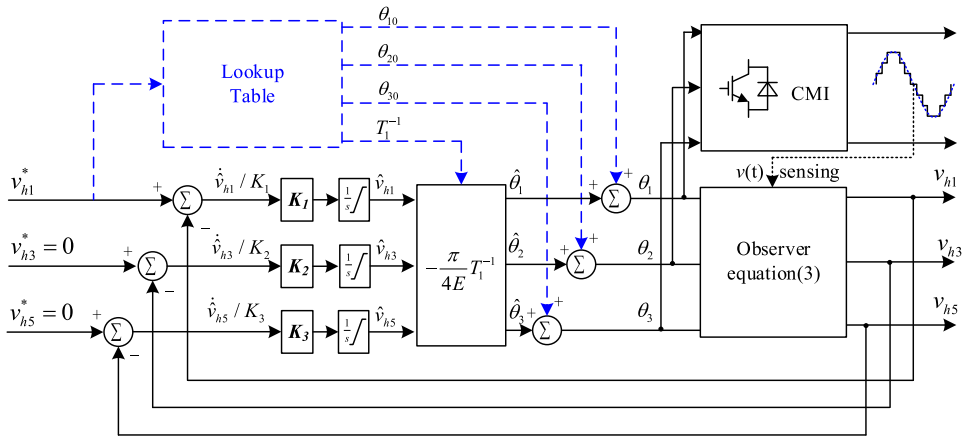

Fig. 21. Extra feedback from sensed output voltage v(t) to observer helps to suppress the unbalanced dc bus voltages.

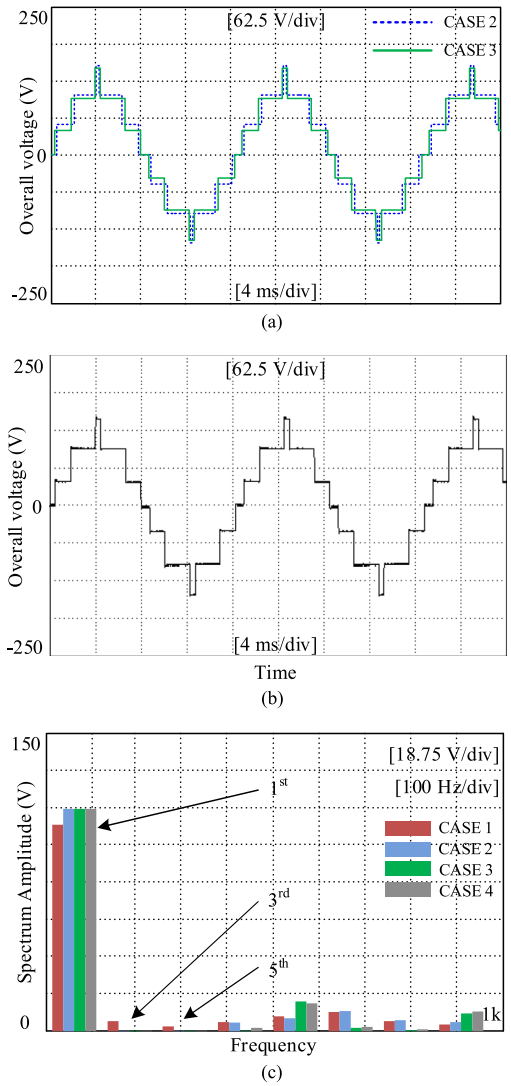

Fig. 22. Simulated and measured steady-state results using the proposed technique in a three-cell CMI with unbalanced dc bus voltages. (a) Overall voltage waveforms with different dc bus voltage conditions, (b) Case 4: a measured output voltage waveform with unbalanced DC bus voltages, voltage feedback and the proposed control loop and (c) FFT results of the voltage waveforms.

have identical length to achieve the minimum peak values and therefore minimum saturation limits. Under this condition, the relationship between the segment peak value θ_{pk} and the number N_p of segments is given by

$$\theta_{pk} = \frac{2.0 - 1.65}{N_p}. \tag{22}$$

Furthermore, from (20) equation (23) as shown at the bottom of the next page.

In (23), with infinite number of segments, all z_i are zero, the matrix reduces to $\begin{bmatrix} -K_1 & 0 & 0 \\ 0 & -K_2 & 0 \\ 0 & 0 & -K_3 \end{bmatrix}$; hence the eigenvalues are λ_1, λ_2 and λ_3; With finite number of segments, there is perturbation on the matrix $\begin{bmatrix} -K_1 & 0 & 0 \\ 0 & -K_2 & 0 \\ 0 & 0 & -K_3 \end{bmatrix}$, the corresponding eigenvalues are μ_1, μ_2 and μ_3. Because the perturbation on the matrix is limited by saturation limits, the perturbation of eigenvalues is also limited [16].

The saturation upper limit is equal to the segment peak value θ_{pk} plus a margin as shown in Fig. 9(c). The lower limit is also equal to the peaks values $\hat{\theta}_2$ and $\hat{\theta}_3$ of plus a margin. At the outputs of the integration function blocks in Fig. 8, the perturbations of eigenvalues are limited by [16]

$$\max|\lambda_i - \mu_i| \le 5.68\sqrt{3}\max(K_i)\left\|T_l^{-1}\right\|\theta_{pk}, \quad \text{where } i = 1, 2, 3. \tag{24}$$

In (24), with $K_1 = K_2 = K_3 = 1000$ and the maximum $\left\|T_l^{-1}\right\| = 2.324$ as shown in Fig. 23 and $\max|\lambda_i - \mu_i| \le 22627\theta_{pk}$. To ensure system is stable, $\max|\lambda_i - \mu_i| \le 22627\theta_{pk} < 1000$, then $\theta_{pk} < 0.044$. Based on (22), $Np \ge 8$.

Because θ_{pk} is overestimated in (23), N_p should be rechecked and adjusted to get the minimum N_P following the process in Fig. 24. For the example in this paper, the minimum Np is found to be 4 finally.

It should be pointed out that, the process to determine the minimum Np is done offline, it has no any bad influence to the real-time operation of the system.

TABLE II
PROPOSED TECHNIQUE IS APPLIED TO A CMI WITH UNBALANCED DC BUS VOLTAGES

	Dc voltage	Theta (rad)	Harmonics (V)
Case 1 (Simulation) unbalanced dc voltage without feedback loop	$E1 = 40$ V (-20%)	$\theta_1 = 0.2044$	1st = 103.1
	$E2 = 55$ V (10%)	$\theta_2 = 0.7737$	3rd = 5.224
	$E3 = 50$ V (0%)	$\theta_3 = 1.5253$	5th = 2.012
Case 2 (Simulation) balanced dc voltage	$E1 = 50$ V	$\theta_1 = 0.2044$	1st = 110.7
	$E2 = 50$ V	$\theta_2 = 0.7737$	3rd = 0
	$E3 = 50$ V	$\theta_3 = 1.5253$	5th = 0
Case 3 (Simulation) unbalanced dc voltage with feedback loop	$E1 = 40$ V (-20%)	$\theta_1 = 0.1265$	1st = 110.7
	$E2 = 55$ V (10%)	$\theta_2 = 0.6751$	3rd = 0
	$E3 = 50$ V (0%)	$\theta_3 = 1.4830$	5th = 0
Case 4 (Experiment) unbalanced dc voltage with feedback loop	$E1 = 40.46$ V (-20%)	$\theta_1 = 0.1306$	1st = 110.7
	$E2 = 54.72$ V (10%)	$\theta_2 = 0.6792$	3rd = 0
	$E3 = 49.96$ V (0%)	$\theta_3 = 1.4847$	5th = 0

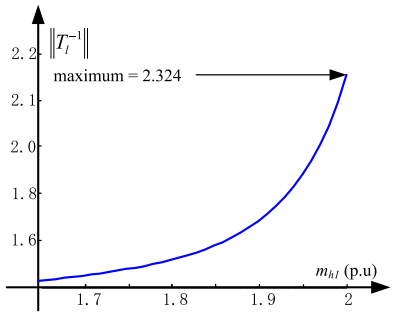

Fig. 23. Frobenius norm of T_l^{-1} as a function of m_{h1}.

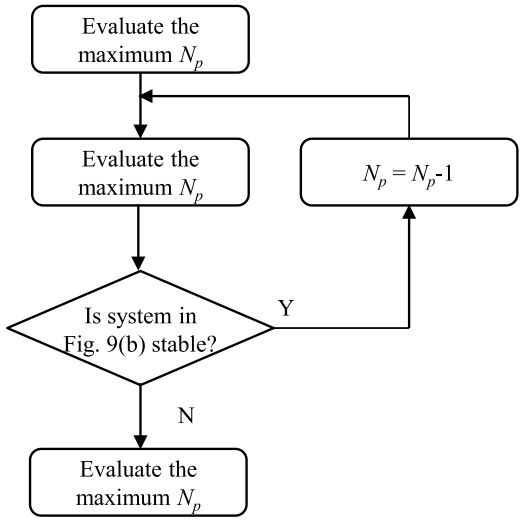

Fig. 24. Flow chart to find the minimum N_P and saturation limits.

E. Comparison of the Memory Space Used by the LUTs With Conventional Technique and the Proposed Technique

The developed technique helps reduce the memory space occupied by LUT. With the modulation range of [1.65–2.0] or an equivalent voltage range of [105 V, 127.3 V] and a voltage accuracy of 0.13 V, for conventional LUT, the number of voltage points should be $(127.3 - 105.0)/0.13 + 1 = 173$. Every point has three data stored for three cells, so total 519 data should be stored in the memory. On the other hand, for the LUT with the proposed technique, the number of voltage points is four, because each point has three data stored, so total 12 data should be stored. Furthermore, each point should have nine data stored for the $3 \times 3\, T_l^{-1}$ matrix which results in 36 data. So, finally, total 48 data are stored in the memory. Table III compares the number of data stored in the memory. The memory space occupied by LUT is greatly reduced by 91% with the proposed technique. When more number of cells are cascaded in CMI or higher voltage accuracy is demanded, the memory space saving would be more significant.

$$
\begin{aligned}
\dot{\hat{v}}_h &= \begin{bmatrix} -K_1 & 0 & 0 \\ 0 & -K_2 & 0 \\ 0 & 0 & -K_3 \end{bmatrix} T_1^{-1} \begin{bmatrix} \sin(\theta_{10}+z_1) & \sin(\theta_{20}+z_2) & \sin(\theta_{30}+z_3) \\ \sin(3(\theta_{10}+z_1)) & \sin(3(\theta_{20}+z_2)) & \sin(3(\theta_{30}+z_3)) \\ \sin(5(\theta_{10}+z_1)) & \sin(5(\theta_{20}+z_2)) & \sin(5(\theta_{30}+z_3)) \end{bmatrix} \hat{v}_h \\
&\approx \begin{bmatrix} -K_1 & 0 & 0 \\ 0 & -K_2 & 0 \\ 0 & 0 & -K_3 \end{bmatrix} T_1^{-1} \left(\begin{bmatrix} \sin(\theta_{10}) & \sin(\theta_{20}) & \sin(\theta_{30}) \\ \sin(3(\theta_{10})) & \sin(3(\theta_{20})) & \sin(3(\theta_{30})) \\ \sin(5(\theta_{10})) & \sin(5(\theta_{20})) & \sin(5(\theta_{30})) \end{bmatrix} + \begin{bmatrix} z_1 & z_2 & z_3 \\ 3z_1 & 3z_2 & 3z_3 \\ 5z_1 & 5z_2 & 5z_3 \end{bmatrix} \right) \hat{v}_h \\
&= \begin{bmatrix} -K_1 & 0 & 0 \\ 0 & -K_2 & 0 \\ 0 & 0 & -K_3 \end{bmatrix} \left(I + T_1^{-1} \begin{bmatrix} z_1 & z_2 & z_3 \\ 3z_1 & 3z_2 & 3z_3 \\ 5z_1 & 5z_2 & 5z_3 \end{bmatrix} \right) \hat{v}_h
\end{aligned} \tag{23}
$$

TABLE III
COMPARISON OF THE OCCUPIED MEMORY SPACE

	Number of voltage points	Number of data
Conventional LUT	173	519
LUT with proposed method	4	48

F. Design of K_1, K_2 and K_3

For the system with only a feedback loop but without a decoupled controller, the controller structure is simple, but its dynamic response is hard to determine because the inputs and outputs would affect each other. Because of this, only the final structure proposed in Section IV will addressed here. The design of K_1, K_2 and K_3 is determined by the dynamic response requirements described in Section IV.

Based on the stability analysis in Section III, parameters K_1, K_2 and K_3 are not critical parameters for system's stability. So the design is simply based on dynamic response requirements. The systems' dynamic response is described in (21). The difference *ER* between the steady-state value and the transient value is given by

$$ER = [(V_2 - V_{20}) - (V_1 - V_{10})]\, e^{-Kt} \leq 0.0875\frac{4}{\pi}Ee^{-Kt}. \tag{25}$$

Because $(V_2 - V_{20}) - (V_1 - V_{10}) \in [-0.0875\frac{4}{\pi}E,\ 0.0875\frac{4}{\pi}E]$, the maximum dynamic error is $0.0875\frac{4}{\pi}E$. The maximum magnitude of fundamental is given by (3) when $\theta n = 0$ in Fig. 1. If *ER* is required to be 0.1% of the maximum magnitude of fundamental at time t_s, then

$$\begin{aligned} 0.0875\frac{4}{\pi}Ee^{-Kt_S} &= 3\frac{4E}{\pi}0.1\% \\ \Rightarrow K &= \frac{3.37}{t_S}. \end{aligned} \tag{26}$$

If $ts = T/5$, then $K \approx 1000$. It is obvious that higher K would decrease the settling time. However, *K* is not the higher, the better because of the quantization errors [17] introduced in DSP and the measurement error susceptibility [18]. On the other hand, conventionally, the settling time should not be larger than T/5 – T/3 for enough margin needed for contingencies such as unbalance dc bus voltage because the switching angle will not be updated until the next fundamental period.

VII. CONCLUSION

This paper proposes a technique to achieve a real-time, transient free inner control loop for SHE applications. The proposed technique converts a transcendental equation set to a MIMO controlled system. The paper discusses the technique to design integral controllers, an instantaneous inner observer and a decoupling controller so as to quickly reach zero steady-state error. Simulation and experimental results verify the proposed technique. The developed technique can be applied to various CMI applications.

REFERENCES

[1] G. S. Konstantinou, M. Ciobotaru, and V. G. Agelidis, "Operation of a modular multilevel converter with selective harmonic elimination PWM," in *Proc. Power Electron. ECCE Asia Int. Conf.*, 2011, pp. 999–1004.

[2] S. Tuncer and Y. Tatar, "An application of SHEPWM technique in a cascade multilevel inverter," *COMPEL: Int. J. Comput. Math. Electr. Electron. Eng.*, vol. 24, pp. 81–93, 2005.

[3] J. Chiasson, L. M. Tolbert, K. McKenzie, and D. Zhong, "A complete solution to the harmonic elimination problem," in *Proc. Appl. Power Electron. Conf. Expo.*, 2003, pp. 596–602.

[4] S. Du, J. Liu, and T. Liu, "A new close-loop based capacitor voltage control method for modular multilevel converter with the switching frequency of 150 Hz," in *Proc. Future Energy Electron. Conf.*, 2013, pp. 426–430.

[5] W. Jin and D. Ahmadi, "A precise and practical harmonic elimination method for multilevel inverters," *IEEE Trans. Ind. Appl.*, vol. 46, no. 2, pp. 857–865, Mar./Apr. 2010.

[6] J. N. Chiasson, L. M. Tolbert, K. J. McKenzie, and D. Zhong, "A complete solution to the harmonic elimination problem," *IEEE Trans. Power Electron.*, vol. 19, no. 2, pp. 491–499, Mar. 2004.

[7] D. Ahmadi and W. Jin, "Online selective harmonic compensation and power generation with distributed energy resources," *IEEE Trans. Power Electron.*, vol. 29, no. 7, pp. 3738–3747, Jul. 2014.

[8] B. Ozpineci, L. M. Tolbert, and J. N. Chiasson, "Harmonic optimization of multilevel converters using genetic algorithms," *IEEE Power Electron. Lett.*, vol. 3, no. 3, pp. 92–95, Sep. 2005.

[9] L. Yu, H. Hoon, and A. Q. Huang, "Real-time calculation of switching angles minimizing THD for multilevel inverters with step modulation," *IEEE Trans. Ind. Electron.*, vol. 56, no. 2, pp. 285–293, Feb. 2009.

[10] H. K. Khalil, *Nonlinear Systems*. Englewood Cliffs, NJ, USA: Prentice Hall, 2002.

[11] G. F. Franklin, J. D. Powell, and A. Emami-Naeini, *Feedback Control of Dynamic Systems*. Singapore: Pearson Education, 2002.

[12] S. Wang, R. Crosier, and Y. Chu, "Investigating the power architectures and circuit topologies for megawatt superfast electric vehicle charging stations with enhanced grid support functionality," in *Proc. IEEE Int. Electric Vehicle Conf.*, Mar. 2012, pp. 1–8.

[13] V. G. Agelidis, A. I. Balouktsis, and M. S. A. Dahidah, "A five-level symmetrically defined selective harmonic elimination PWM strategy: Analysis and experimental validation," *IEEE Trans. Power Electron.*, vol. 23, no. 1, pp. 19–26, Jan. 2008.

[14] A. Edpuganti and A. K. Rathore, "Optimal low switching frequency pulsewidth modulation of nine-level cascade inverter," *IEEE Trans. Power Electron.*, vol. 30, no. 1, pp. 482–495, Jan. 2015.

[15] B. Ozpineci, L. M. Tolbert, and J. N. Chiasson, "Harmonic optimization of multilevel converters using genetic algorithms," *IEEE Power Electron. Lett.*, vol. 3, no. 3, pp. 92–95, Sep. 2005.

[16] J. Sun., "Perturbation analysis for the generalized singular value problem," *SIAM J. Numerical Anal.*, vol. 20, no.3, pp. 611–625, 1983.

[17] A. V. Oppenheim and R. W. Schafer, *Discrete-Time Signal Processing*. Englewood Cliffs, NJ, USA: Prentice Hall, 2009.

[18] K. J. Åström and B. Wittenmark, *Computer-Controlled Systems: Theory Design*. New York, NY, USA: Dover, 2011.

[19] H. Liqun, Z. Kai, X. Jian, and F. Shengfang, "A repetitive control scheme for harmonic suppression of circulating current in modular multilevel converters," *IEEE Trans. Power Electron.*, vol. 30, no. 1, pp. 471–481, Jan. 2015.

Hui Zhao (S'14) received the bachelor's and master's degrees in electrical engineering from the Huazhong University of Science and Technology, Wuhan, China, in 2010 and 2013, respectively. He is currently working toward the Ph.D. degree at the Electrical and Computer Engineering Department, University of Florida, Gainesville, FL, USA.

He had a summer internship at General Electric Global Research Center Shanghai in 2013. He has authored and coauthored several IEEE conference and transaction papers.

Tian Jin received the Master degree in electrical engineering from the University of Texas at San Antonio, San Antonio, TX, USA, in 2014.

His current research interests include power system modeling and electrical magnetic interference.

Shuo Wang (S'03–M'06–SM'07) received the Ph.D. degree from Virginia Tech, Blacksburg, VA, USA, in 2005.

He has been with the Department of Electrical and Computer Engineering, University of Florida, Gainesville, FL, USA, since 2015. From 2010 to 2014, he was with the University of Texas at San Antonio, first as an Assistant Professor and later as an Associate Professor. From 2009 to 2010, he was a Senior Design Engineer at GE Aviation Systems, Vandalia, OH, USA. From 2005 to 2009, he was a Research Assistant Professor at Virginia Tech. He has published more than 100 IEEE journal and conference papers and holds seven US patents.

Dr. Wang received the Best Transaction Paper Award from the IEEE Power Electronics Society in 2006 and two William M. Portnoy Awards for the papers published in the IEEE Industry Applications Society in 2004 and 2012, respectively. In 2012, he received the prestigious National Science Foundation CAREER Award. He is an Associate Editor for the IEEE TRANSACTIONS ON INDUSTRY APPLICATIONS and a Technical Program Cochair for IEEE 2014 International Electric Vehicle Conference.

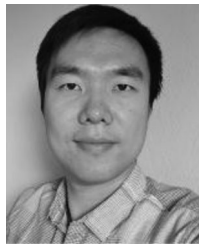

Liang Sun received the B.S. and M.S. degrees in automation science and electrical engineering from Beihang University, Beijing, China, in 2004 and 2007, respectively. In 2012, he received the Ph.D. degree in electrical and computer engineering from Brigham Young University, Provo, UT, USA.

He is currently working as a Postdoctoral Research Fellow at the Unmanned Systems Laboratory, Department of Electrical and Computer Engineering, University of Texas at San Antonio, San Antonio, TX, USA. His research interests include unmanned aircraft systems, towed-cable systems, dynamic modeling, motion planning, nonlinear control, optimal control, and cooperative control.